

Object-Attribute-Relation Representation based Video Semantic Communication

Qiyuan Du, *Student Member, IEEE*, Yiping Duan, *Member, IEEE*, Qianqian Yang, *Member, IEEE*, Xiaoming Tao, *Member, IEEE*, and Mérouane Debbah, *Fellow, IEEE*,

Abstract—With the rapid growth of multimedia data volume, there is an increasing need for efficient video transmission in applications such as virtual reality and future video streaming services. Semantic communication is emerging as a vital technique for ensuring efficient and reliable transmission in low-bandwidth, high-noise settings. However, most current approaches focus on joint source-channel coding (JSCC) that depends on end-to-end training. These methods often lack an interpretable semantic representation and struggle with adaptability to various downstream tasks. In this paper, we introduce the use of object-attribute-relation (OAR) as a semantic framework for videos to facilitate low bit-rate coding and enhance the JSCC process for more effective video transmission. We utilize OAR sequences for both low bit-rate representation and generative video reconstruction. Additionally, we incorporate OAR into the image JSCC model to prioritize communication resources for areas more critical to downstream tasks. Our experiments on traffic surveillance video datasets assess the effectiveness of our approach in terms of video transmission performance. The empirical findings demonstrate that our OAR-based video coding method not only outperforms H.265 coding at lower bit-rates but also synergizes with JSCC to deliver robust and efficient video transmission.

Index Terms—Video Coding, Object-Attribute-Relation, Wireless Transmission, Joint Source-Channel Coding, Semantic Communication.

I. INTRODUCTION

This work was supported by the National Natural Science Foundation of China (Nos. NSFC 61925105, 62227801, 62322109, 62171257 and U22B2001), State Key Laboratory of Space Network and Communications, New Cornerstone Science Foundation through the XPLOER PRIZE, and the Tsinghua University (Department of Electronic Engineering)-Nantong Research Institute for Advanced Communication Technologies Joint Research Center for Space, Air, Ground and Sea Cooperative Communication Network Technology. (*Corresponding author: Xiaoming Tao.*)

Qiyuan Du, Yiping Duan and Xiaoming Tao are with the Department of Electronic Engineering, Tsinghua University, Beijing, China, and also with the State Key Laboratory of Space Network and Communications, Beijing, China (email: dqy21@mails.tsinghua.edu.cn, yiping-duan@mail.tsinghua.edu.cn, taoxm@mail.tsinghua.edu.cn).

Qianqian Yang is with College of Information Science and Electronic Engineering, Zhejiang University, Hangzhou, China (email: qianqianyang20@zju.edu.cn).

Mérouane Debbah is with the KU 6G Research Centre, Khalifa University of Science and Technology, Abu Dhabi, United Arab Emirates, and also with CentraleSupélec, Paris-Saclay University, 91192 Gif-sur-Yvette, France (e-mail: merouane.debbah@ku.ac.ae).

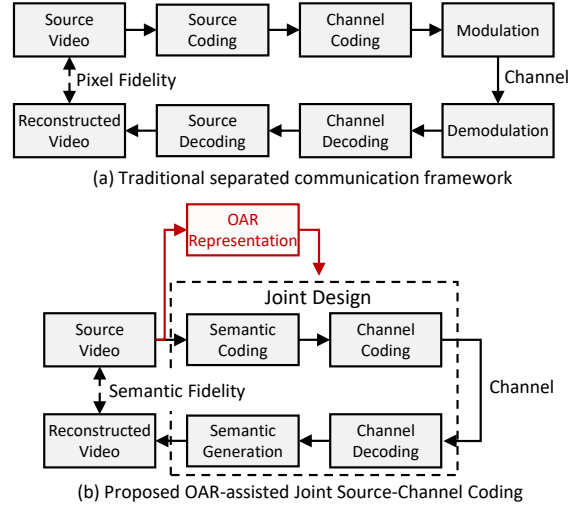


Fig. 1. Comparison between traditional communication, classical semantic communication (without the OAR representation module) and the proposed OAR-based video transmission frameworks.

AS video services increasingly dominate the multimedia traffic, the need for low bit-rate video compression and efficient transmission is becoming more critical. Traditional methods typically use a separate source-channel coding strategy to ensure pixel and symbol accuracy, as illustrated in Figure 1 (a). However, with diminishing returns from standard video encoders [1], the video quality at low bit-rates fails to satisfy user perception and task-specific requirements. Moreover, the distinct separation of source and channel coding can jeopardize the reliable transmission of video, especially over channels with low signal-to-noise ratios (SNRs), leading to increased instances of decoding failures [2].

Semantic communication [3] is emerging as a pivotal framework capable of surpassing the Shannon limit. By focusing on the semantic level of data characterization and transmission, it moves beyond traditional bit and symbol constraints, enhancing task-specific communication performance [4]. With the support of deep learning technologies [5], semantic communication has advanced significantly in both theory and practice, outperforming conventional communication methods in various appli-

cations [6]–[10].

Semantic information extraction and joint source-channel coding (JSCC) are crucial for semantic communication systems aiming for efficient transmission. By enabling effective semantic representations, these systems can prioritize critical semantic information (e.g., by allocating more bits or transmitted symbols) to enhance transmission efficiency. Recent advancements in image coding using semantic representations have shown promising results [8], [11]. Additionally, leveraging deep learning, deep JSCC methods have been developed and shown to outperform traditional separate coding frameworks in transmission performance [2], [12]–[15]. Notably, for structured multimedia such as audio and video, JSCC methods have achieved efficient transmission even at low signal-to-noise ratios (SNRs), significantly reducing the time and bandwidth costs caused by decoding failures. An overview of the JSCC framework is depicted in Figure 1 (b).

Research into explicit semantic representation and transmission of videos is still limited. Studies such as [16]–[20] have explored using semantic segmentation maps and scene graphs for semantic representations, implementing corresponding image and video generation to preserve the videos’ semantic content. However, these studies did not deeply engage with compression perspectives or data volume reduction. In [8], [21], [22], semantic segmentation maps served as explicit semantic representations for image compression, enhancing semantic fidelity by varying bit-rates across different categories. These efforts treated semantic information as supplementary to traditional image compression, relying still on transmitting numerous pixel and residual features for quality enhancements, which hindered significant bit-rate reductions. [23] took a different approach by encoding and transmitting only semantic segmentation maps and reconstructing images using a diffusion model, catering to extreme channel conditions. Similarly, [11] used sketch representations and generative models. In video conferencing, efficient transmission was achieved using facial keypoints [24]. Nevertheless, these approaches primarily focused on the semantic representation and coding of images or simpler video formats. The challenge remains to explore these techniques for large-scale, time-continuous, and object-consistent video representation to fully address the complexities of large scene videos.

Several JSCC approaches have been proposed for video transmission, yet there remains a dearth of research delving into explicit semantic representation and extraction of video contents. Approaches like DeepWive [14] and [25] have achieved residual estimation based video transmission by employing bidirectional optical flow estimation, along with channel bandwidth allocation

among frames. DVST [9] and MDVSC [26] have utilized nonlinear transforms and shared prior distributions for channel bandwidth allocation in features. However, these endeavors have predominantly focused on implicit latent features which are usually outputs of some neural layers. While ABRVSC [27] instead transmits category labels of videos frames for video sensing tasks, the receiver however can only recover category labels, resulting in a loss of significant video contents when adopted for video reconstruction. Thus, reliable video transmission with explicit semantic representation and extraction needs to be further explored.

To address the above issues, this paper proposes a novel video transmission system leveraging object-attribute-relation (OAR) representation model of semantic information, as shown in Fig. 1 (b). Specifically, object-attribute-relation (OAR) model characterizes scene semantics by capturing key objects and their attributes and relations of video frames with regards to downstream application requirements. Compared with object edges and semantic segmentation maps widely used in previous studies, OAR captures more structured semantic correlations, which are represented by connected graphs; compared with scene graph representation, OAR pays more attention to the enrichment of attributes, which enables better reconstruction of videos. In addition, this paper implements a JSCC pipeline for video transmission by exploiting the advantages of compact and downstream tasks related OAR data. Specifically, this paper implements OAR-assisted JSCC for key frames so that the model can pay more attention to the key objects in the scene. Experimental validation is performed on traffic surveillance videos, and the results indicate that the proposed system can still maintain better foreground reconstruction quality under low bandwidth and SNR conditions.

In summary, the contributions of this paper include the following:

- 1) We propose an OAR-based video representation and generative reconstruction system for video transmission. In particular, OAR graphs characterize the motion and state changes of objects in a video, enabling low bit-rate video coding. This preserves foreground objects and semantics even at low bit-rates, thus overcoming the performance degradation of traditional video encoders for downstream tasks.
- 2) We propose an OAR-assisted JSCC method for the transmission of key video frames. This method uses OAR as the side information to the channel coding and image reconstruction process, which leads to the enhancement of perceptual quality; For non-key video frames, we transmit only OAR representations.

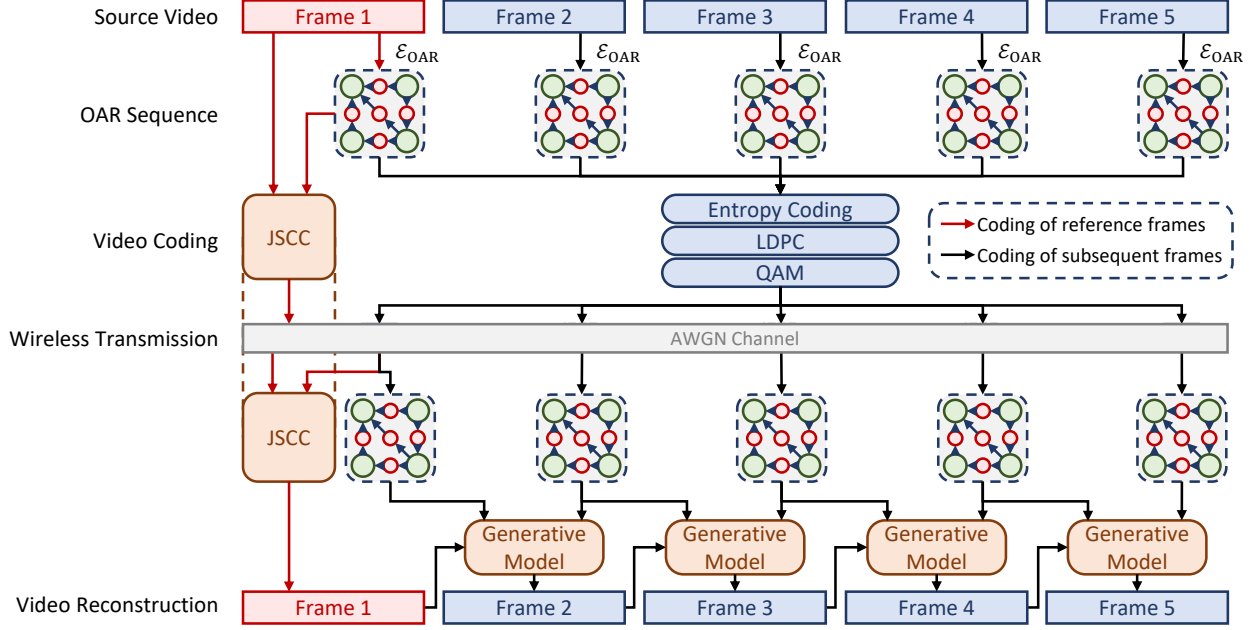


Fig. 2. Overall framework of OAR-based video compressive coding and transmission. Frames are represented by OAR and transmitted via LDPC channel coding and QAM modulation. Additionally, the reference frame is coded and transmitted via OAR-assisted JSCC.

3) Experiments on a traffic surveillance dataset show that the proposed method improves the perceptual quality of reconstructed videos significantly compared to conventional methods such as H.265 and prior work in semantic communication, namely DVST. Specifically, at a CBR of 1/300, the proposed method exhibits an average reduction in LPIPS loss of 0.037 when compared to DVST. Additionally, it facilitates improved performance in object detection tasks, achieving an average increase in mean average precision (mAP) of 0.16 compared to DVST.

The remainder of this paper is organized as follows: in section II, we introduce the OAR-based video coding and reconstruction method. In section III, OAR-based image JSCC system is introduced, and a video transmission system that combines OAR representation and image JSCC is presented. Section IV includes the experimental design and the results of the OAR-based video coding method and the transmission system. Section V includes the analysis, discussion and ablation studies. Section VI summarizes the entire paper.

II. OBJECT-ATTRIBUTE-RELATION-BASED VIDEO REPRESENTATION AND CODING

A. Object-Attribute-Relation Formulation and OAR Based Video Communication Framework

An Object-Attribute-relation (OAR) representation is a structured abstraction of the scene semantics in

the form of a graph. For image \mathbf{I} , the OAR is expressed as a tuple of objects, attributes and relations: $\mathbf{I} \xrightarrow{\mathcal{E}_{OAR}} (\mathcal{O}, \mathcal{A}, \mathcal{R})$, where \mathcal{E}_{OAR} denotes the mapping from the image to OAR. For video frames, the OAR is represented as a temporal sequence, $[(\mathcal{O}_1, \mathcal{A}_1, \mathcal{R}_1), \dots, (\mathcal{O}_T, \mathcal{A}_T, \mathcal{R}_T)]$.

As shown in the formula, OAR contains three components: $\mathcal{O} = [o_1, \dots, o_N]$, $\mathcal{A} = [\mathbf{a}_1, \dots, \mathbf{a}_N]$, and $\mathcal{R} = \{r_1, \dots, r_K\}$, where N, K denote the numbers of objects and relations, respectively. \mathcal{O} is the object set with o_n denoting a unique ID for each object. \mathcal{A} is the attribute set, with $\mathbf{a}_n = (a_1^{(n)}, a_2^{(n)}, \dots, a_A^{(n)}) = \mathcal{E}_A(\mathbf{I}, o_n)$ denoting A attributes of object o_n . The relation is denoted by $\mathcal{R} = \{\mathbf{r}_1, \dots, \mathbf{r}_K\} = \{(o_{s,1}, o_{o,1}, r_1), \dots, (o_{s,K}, o_{o,K}, r_K)\}$, $r_k = r_{o_{s,k} \rightarrow o_{o,k}}$ representing the relation with subject $o_{s,k}$ and object $o_{o,k}$. An OAR is characterized by a directed graph with objects as nodes and relations as edges. The relations and attributes (e.g., category, color, etc.) take values from a deterministic set, i.e.,

$$\begin{aligned} a_p^{(n)} &\in \mathcal{A}_p, p = 1, 2, \dots, A \\ r_{o_i \rightarrow o_j} &\in \mathcal{R}, i, j = 0, 1, 2, \dots, N. \end{aligned} \quad (1)$$

OAR is highly interpretable and has a small data volume because only semantics of key objects are characterized. It is especially conducive to task-oriented applications with steady backgrounds, such as surveillance videos. Additionally, OAR provides scalability and can be adapted to more complex scenarios through the

extension of attributes and relations. Based on the above formulation, this paper proposes an OAR-based video transmission framework, as presented in Fig. 2.

In the proposed framework, T consecutive frames are encapsulated as one group-of-pictures (GoP). The first frame of each GoP (reference frame or key frame) is intra-coded and transmitted, providing contour and texture information about the background and key objects. OAR sequences are extracted for subsequent frames and transmitted. The receiver carries out generative reconstruction based on the reference frame incorporated with OAR sequences. Without loss of generality, each GOP is independently processed. Reference frames are denoted by \mathbf{I}_1 , while subsequent $T - 1$ frames are denoted by $\mathbf{I}_t, t = 2, \dots, T$. For objects contained in reference frames, faithful reconstruction is realized based on the motion information in OAR. Newly appeared objects are generated based on the prior knowledge of the trained models, resulting in possible bias in details such as colors and textures. This paper focuses on task-oriented video transmission, so deviation in detailed textures are acceptable under the premise of semantic fidelity.

B. OAR Formulation and Extraction

OAR representation is the critical component of the proposed video transmission system, providing semantics for low bit-rate representation and enabling efficient video transmission. Considering a surveillance video transmission system oriented towards tasks such as object detection and anomaly monitoring. Vehicles in the foreground are treated as the objects in OAR. Attributes consist of the position $\mathbf{p} = (x, y)$, size $\mathbf{s} = (w, h)$, angle θ , and category c , denoted by $\mathbf{a} = (a_1, a_2, a_3, a_4) = (\mathbf{p}, \mathbf{s}, \theta, c)$. Relations involve mainly “occlusions” between foreground objects and occlusions of the foreground by the background. The trivial relation of objects “in” the background is also included. Consequently, for an image of size $W \times H$, the attributes and relations take the value space of:

$$\begin{aligned} \mathbf{p}, \mathbf{s} &\in \mathcal{A}_1 = \mathcal{A}_2 = [0, W] \times [0, H] \\ \theta &\in \mathcal{A}_3 = [0, 360] \\ c &\in \mathcal{A}_4 = \{\text{car, bus, van, others, background}\} \\ r_{o_i \rightarrow o_j} &\in \mathcal{R} = \{\text{occlusion, in, null}\}. \end{aligned} \quad (2)$$

To realize automated OAR extraction, multi-object tracking (MOT) is utilized, followed by several attribute recognition models. The overall process mainly consists of three parts: multi-object tracking, attribute recognition, and relation identification.

First, multi-object tracking. Object detection is first conducted via YOLOv9 [28] to obtain the categories $c_n^{(t)}$ and bounding boxes $\mathbf{b}_n^{(t)} = (x_n^{(t)}, y_n^{(t)}, w_n^{(t)}, h_n^{(t)})$, where $n = 1, \dots, N_t$. To match the identical objects in

consecutive frames, a unique ID $o_n^{(t)}$ is assigned to each object via SORT [29]. IDs for all objects constitute the object component $\mathcal{O}_t = [o_1^{(t)}, \dots, o_{N_t}^{(t)}]$ in OAR.

Second, attribute recognition. The object pose, i.e., orientation $\theta_n^{(t)}$ in the 2D pixel plane, is estimated via an angle estimation network EgoNet [30]. Combined with the category and bounding box, they collectively constitute the attribute component in the OAR: $\mathcal{A}_t = [\mathbf{a}_1^{(t)}, \dots, \mathbf{a}_{N_t}^{(t)}]$, where $\mathbf{a}_n^{(t)} = (\mathbf{p}_n^{(t)}, \mathbf{s}_n^{(t)}, \theta_n^{(t)}, c_n^{(t)})$.

Third, relation identification. The occlusion relation is determined among object pairs with intersecting bounding boxes by comparing the appearance of the overlapping regions with the respective object features. Besides, occlusions between objects and background elements are also considered. Regions located at the spatial forefront are manually labeled. Objects overlapping with the labeled area are considered to be occluded by the background. Incorporating the identified “occlusion” and the trivial “in” relation, the relation component in OAR is formulated by $\mathcal{R}_t = \{\mathbf{r}_1^{(t)}, \dots, \mathbf{r}_K^{(t)}\}$.

C. OAR Based Video Generative Reconstruction

At the receiver, generative reconstruction is conducted based on the received OAR sequence combined with reference frames. The overall framework is shown in Fig. 3, which can be divided into four modules: (1) OAR embedding and graph computing, (2) OAR layout generation, (3) optical flow estimation and frame prediction, and (4) image synthesis and fusion. Because the OAR for each video frame is processed by the same process of OAR embedding, graph computing and layout generation, the time superscripts have been omitted in modules (1) and (2) for brevity.

1) *OAR Embedding and Graph Computing*: The category c_n , angle θ_n (quantized by q -bits) and relation r_k are first represented by one-hot vectors $\mathbf{c}_n, \boldsymbol{\theta}_n, \mathbf{r}_k$. Three projection matrices $\mathbf{W}_c, \mathbf{W}_\theta, \mathbf{W}_r$ are learned to map the vectors into an embedding space [31], denoted by:

$$\begin{aligned} \mathbf{e}_c^{(n)} &= \mathbf{W}_c \mathbf{c} \\ \mathbf{e}_\theta^{(n)} &= \mathbf{W}_\theta \boldsymbol{\theta} \\ \mathbf{e}_r^{(k)} &= \mathbf{W}_r \mathbf{r}. \end{aligned} \quad (3)$$

For the object “background”, the category is embedded based on the same method, and the angle embedding vector is set to a constant $\mathbf{0}$.

A graph convolutional network (GCN, denoted by \mathcal{G}_{OAR}) is utilized with reference to [32] for deep feature extraction of OARs. Specifically, a primary graph is constructed with the concatenation of category and angle embedding vectors $\mathbf{e}^{(n)} = \text{concat}(\mathbf{e}_c^{(n)}, \mathbf{e}_\theta^{(n)})$ as nodes and the relation embedding vectors $\mathbf{e}_r^{(k)}$ as directed edges from $o_{s,k}$ to $o_{o,k}$. Subsequently, the primary graph is

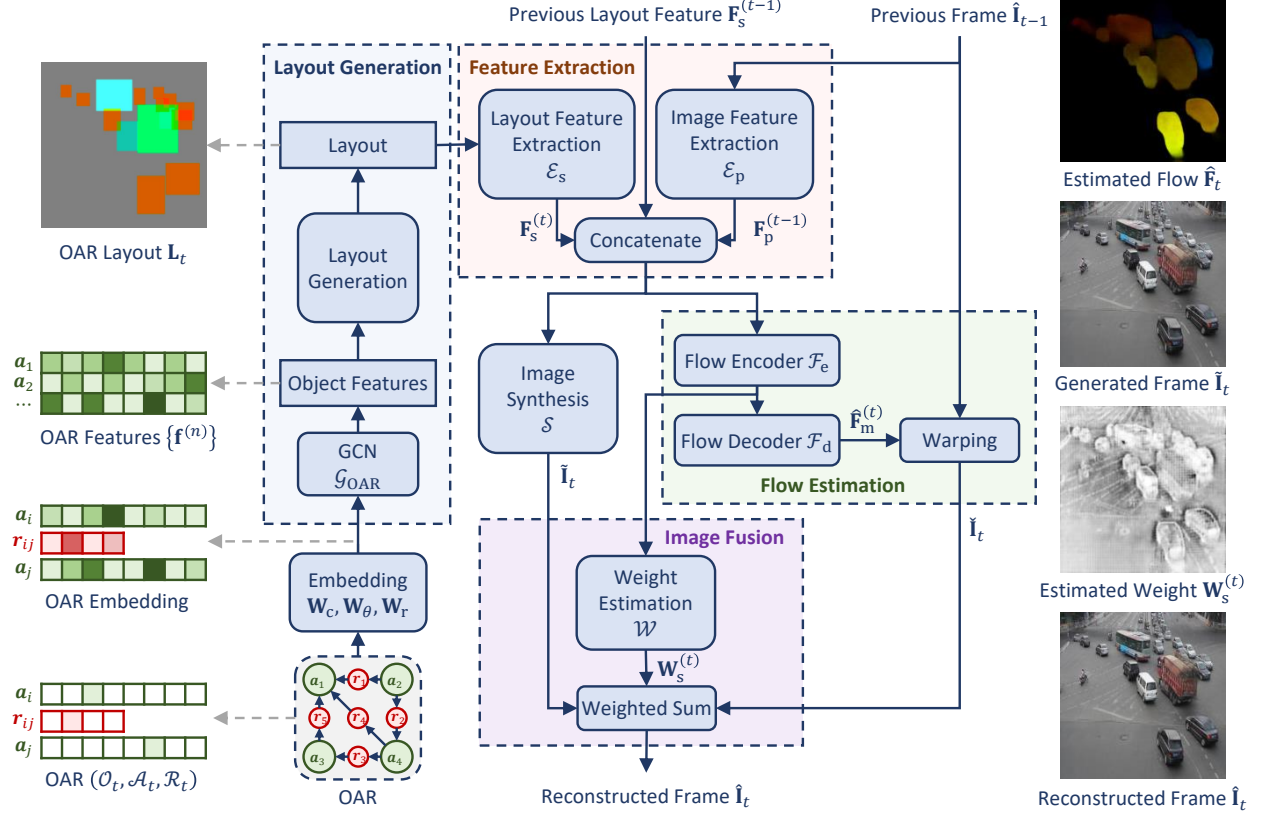


Fig. 3. Framework of OAR-based video generation and visualizations for intermediate results.

processed by a two-layer GCN to obtain a deep feature for each object, denoted by $\mathbf{f}^{(n)}$.

2) *OAR Layout Generation*: Temporal dynamics of the motion and scale evolution of objects are captured by the location and size attributes of the OAR. With reference to AG2Video [20], the feature vector of each object is propagated to obtain the layout feature $\mathbf{L} \in \mathbb{R}^{H \times W \times D}$. The element $\mathbf{L}_{i,j,d}$ is formulated as:

$$\mathbf{L}_{i,j,d} = \sum_{n=1}^N \mathbf{L}_{i,j,d}^{(n)}, \quad (4)$$

where $\mathbf{L}^{(n)} \in \mathbb{R}^{H \times W \times D}$ represents the individual layout of the n -th object. Specifically, the deep feature $\mathbf{f}^{(n)}$ is expanded to the region corresponding to the bounding box $\mathbf{b}_n = (x_n, y_n, w_n, h_n)$, which is computed by:

$$\mathbf{L}_{i,j,d}^{(n)} = \begin{cases} \mathbf{f}_d^{(n)}, & \text{if } y^{(n)} \leq i \leq y^{(n)} + h^{(n)}, \\ & \text{and } x^{(n)} \leq j \leq x^{(n)} + w^{(n)}, \\ 0, & \text{otherwise.} \end{cases} \quad (5)$$

One layout is generated from OAR of each video frame, constructing the layout sequence: $[\mathbf{L}_1, \dots, \mathbf{L}_T]$.

3) *Optical Flow Estimation and Frame Prediction*: With reference frames providing appearance information of objects, primary image prediction is conducted based

on the motion information of OAR via optical flow estimation. The t -th frame ($t \geq 2$) is predicted based on the previous synthesized frame $\hat{\mathbf{I}}_{t-1}$ and adjacent layouts $\mathbf{L}_{t-1}, \mathbf{L}_t$. First, a semantic feature extractor \mathcal{E}_s and a pixel feature extractor \mathcal{E}_p are utilized to obtain deep OAR features of the two frames $\mathbf{F}_s^{(t)} = \mathcal{E}_s(\mathbf{L}_t)$, $\mathbf{F}_s^{(t-1)} = \mathcal{E}_s(\mathbf{L}_{t-1})$, and image features of the previous frame $\mathbf{F}_p^{(t-1)} = \mathcal{E}_p(\hat{\mathbf{I}}_{t-1})$, respectively. Optical flows are then estimated via an optical flow estimator \mathcal{F} in two stages:

$$\begin{aligned} \hat{\mathbf{F}}_m^{(t)} &= \mathcal{F}(\mathbf{F}_s^{(t)}, \mathbf{F}_s^{(t-1)}, \mathbf{F}_p^{(t-1)}) \\ &= \mathcal{F}_d(\mathcal{F}_e(\mathbf{F}_s^{(t)}, \mathbf{F}_s^{(t-1)}, \mathbf{F}_p^{(t-1)})) \\ &\in \mathbb{R}^{H \times W \times 2}. \end{aligned} \quad (6)$$

Based on the estimated optical flows $\hat{\mathbf{F}}_m^{(t)}$, the predicted image can be obtained by $\check{\mathbf{I}}_t = \text{warp}(\hat{\mathbf{I}}_{t-1}, \hat{\mathbf{F}}_m^{(t)})$.

4) *Image Synthesis and Fusion*: While frame prediction enables the reconstitution of object motions, occluded regions and newly emerging objects cannot be resolved. Accordingly, generative reconstruction is employed for detail complementation with reference to vid2vid [19]. Specifically, an image synthesis network \mathcal{S} is implemented to generate the current frame by

$$\tilde{\mathbf{I}}_t = \mathcal{S}(\mathbf{F}_s^{(t)}, \mathbf{F}_s^{(t-1)}, \mathbf{F}_p^{(t-1)}). \quad (7)$$

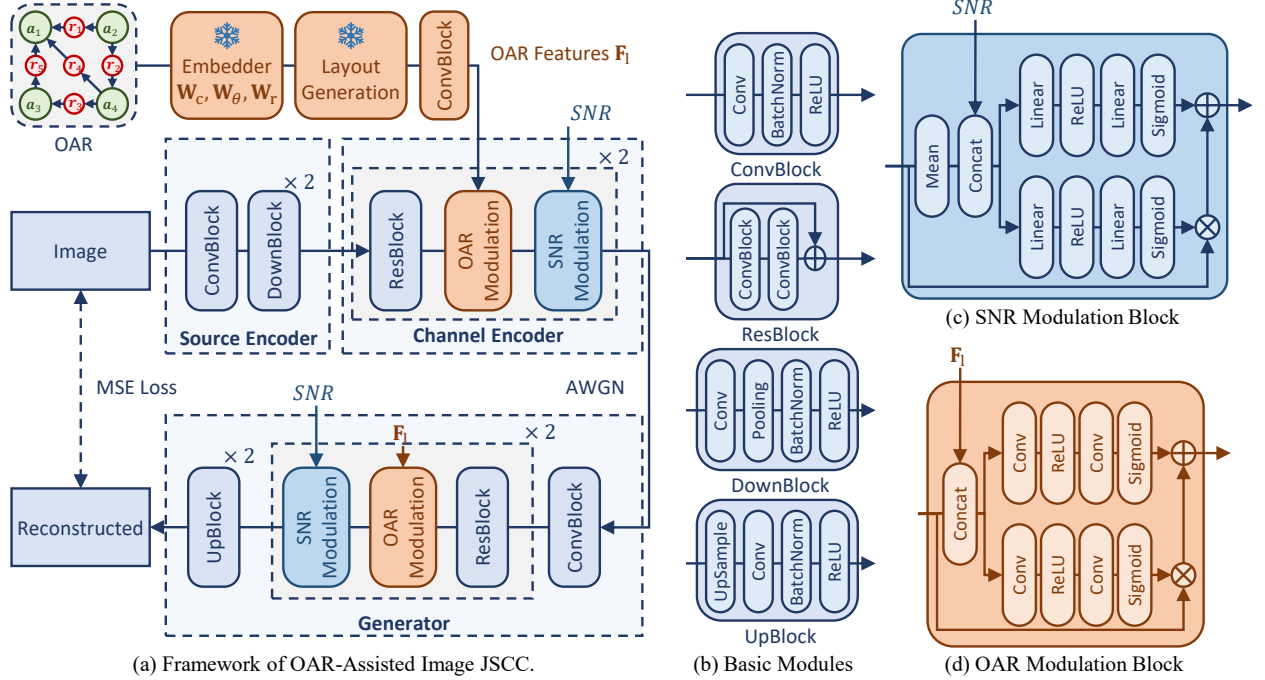


Fig. 4. The framework of OAR-assisted image JSCC. The SNR is assumed to be available at both transmitter and receiver. OAR undergoes lossless transmission, ensuring that both the transmitter and receiver obtain identical OAR features \mathbf{F}_1 through the utilization of OAR feature extraction networks with identical parameters.

Finally, a weight estimation network \mathcal{W} is implemented for mask prediction from optical flow features, denoted by $\mathbf{W}_s^{(t)} = \mathcal{W}(\mathcal{F}_e(\mathbf{F}_s^{(t)}, \mathbf{F}_s^{(t-1)}, \mathbf{F}_p^{(t-1)})) \in [0, 1]^{H \times W}$. The predicted image $\tilde{\mathbf{I}}_t$ and the synthesized image $\hat{\mathbf{I}}_t$ are fused to obtain the final synthesis:

$$\hat{\mathbf{I}}_t = \mathbf{W}_s^{(t)} \odot \tilde{\mathbf{I}}_t + (1 - \mathbf{W}_s^{(t)}) \odot \hat{\mathbf{I}}_t \quad (8)$$

A set of intermediate results is shown in Fig. 3. The layout \mathbf{L}_t , the estimated optical flows $\hat{\mathbf{F}}_m^{(t)}$, the image synthesis results $\tilde{\mathbf{I}}_t$, the estimated weights $\mathbf{W}_s^{(t)}$ and the final generated results $\hat{\mathbf{I}}_t$ are illustrated.

III. OAR-ASSISTED JSCC AND VIDEO TRANSMISSION

In this section, video transmission over Gaussian channels is realized, including transmission of reference frames and OAR sequences. OAR-modulated JSCC is proposed for reference frame transmission with reference to DynamicJSCC [12], and OAR sequences is transmitted via LDPC [33] and QAM.

A. OAR-modulated JSCC

For the coding and transmission of key frames, OAR representation is integrated with Dynamic JSCC [12] as the backbone, consisting of jointly trained source encoder \mathcal{E}_{se} , channel encoder \mathcal{E}_{ce} and generator \mathcal{G} . The

overall framework is shown in Fig. 4 (a). The framework contains two parts: OAR feature extraction and OAR-assisted image JSCC.

The OAR layout \mathbf{L}_1 is first generated through the layout generation method implemented in section II. Afterwards, deep layout features are obtained through a convolutional layer: $\mathbf{F}_1 = \text{Conv}_1(\mathbf{L}_1) \in \mathbb{R}^{H/4 \times W/4 \times C}$.

In the backbone of the JSCC networks, OAR modulation module is introduced into the channel encoder \mathcal{E}_{ce} and generator \mathcal{G} , which is shown in Fig. 4 (d). A set of multiplier $\mathbf{m} \in (0, 1)^{H/4 \times W/4 \times 1}$ and bias $\mathbf{b} \in (0, 1)^{H/4 \times W/4 \times 1}$ is learned from the feature to be modulated \mathbf{F}_{in} and the layout feature \mathbf{F}_1 . The feature distribution is shifted by performing a linear operation:

$$\mathbf{F}_{out} = \mathbf{F}_{in} \odot \mathbf{m} + \mathbf{b} \quad (9)$$

In conjunction with the Gaussian noise \mathbf{n} , the reconstructed image at the receiver can be denoted by:

$$\hat{\mathbf{I}}_1 = \mathcal{G}(\mathcal{E}_{ce}(\mathcal{E}_{se}(\mathbf{I}_1) | \mathbf{L}_1) + \mathbf{n} | \mathbf{L}_1) \quad (10)$$

With OAR-based modulation, the JSCC system enhances object retention by prioritizing foreground regions. Meanwhile, the integration of OAR features into the generator offers additional semantic cues for the decoding of foreground objects, thereby improving adaptability to higher noise levels.

B. OAR-based Video Transmission Pipeline

This section integrates the OAR-based video coding system presented in section II with the OAR-assisted image JSCC to propose an OAR-based video transmission framework. Illustrated in Fig. 2, the framework comprises three components: JSCC of key frames, OAR transmission, and OAR-based video reconstruction. OAR-assisted source and channel coding are applied to key frames for transmission via Gaussian channels. Upon reception, reconstruction from the received symbols yields the reconstructed frame \hat{I}_1 , enabling the restoration of non-key frames. OAR transmission is conducted using 1/3-rate LDPC and 4QAM modulation, which realizes distortion-free transmission. With the received reference frames and OAR sequences, the receiver performs video reconstruction based on the video generation network in II-C.

IV. EXPERIMENTS AND RESULTS

A. Dataset, Performance Metrics and Baselines

1) *Dataset Preparation*: We conduct experiments on the traffic surveillance video dataset UA-DETRAC [34] for performance validation. Given the limitations of current MOT and attribute recognition algorithms in achieving accurate recognition, we utilize the ground truth for subsequent experimental analysis.

Video frames are segmented into a training set and two validation sets with a ratio of 8:1:1 for the number of frames. Validation set `val1` shares the same scenes with the training set but features different objects and motions, facilitating validation of generating diverse objects. Conversely, validation set `val2` comprises distinct scenes from the training set, enabling assessment of performance across different backgrounds.

2) *Experiment Settings*: Models in the proposed framework are trained in two steps. First, the OAR-based video reconstruction model is trained with original reference frames. The loss function, inspired by `vid2vid` [19], imposes constraints on reconstructed video quality across spatial and temporal dimensions. Subsequently, the OAR-based JSCC network is trained on AWGN channels. Symbol amplitudes are normalized to ensure an average signal power of 1, followed by the addition of noise sampled randomly at SNRs ranging from 0 to 20 dB to the transmitted symbols.

Experiments are conducted to validate performance from two perspectives: video coding and wireless transmission. In both scenarios, video reconstruction is realized via the same model in II-C. However, different compression and transmission methods are employed for reference frames. In the video coding task, reference frames undergo compression via BPG [35] and losslessly transmitted to evaluate the performance of the video

reconstruction network. For wireless video transmission, reference frames are transmitted through OAR-assisted JSCC followed by an AWGN channel.

3) *Performance Metrics*: We evaluate performance from perspectives of pixel fidelity, perceptual quality, distribution similarity, and task performance. Specifically, PSNR and SSIM assess pixel fidelity, LPIPS [36] represents perceptual quality, while FID [37] and KID [38] measure distribution similarity. Additionally, mAP serves as a metric for task-level evaluation.

PSNR and SSIM metrics, indicative of pixel-level similarity, are computed using TensorFlow. LPIPS, FID and KID metrics extract deep features through neural networks, measuring feature similarity as the metric. LPIPS and FID (KID) are calculated utilizing open-source codes [36] and [39], respectively.

In addition to the aforementioned metrics, this paper also conducts video quality assessment from a task-oriented perspective using mean average precision (mAP) of object detection tasks. An object detection model is trained on the original video frames, and subsequently applied to perform object detection on the reconstructed videos. The mAP metric is then computed to reflect the video quality. In the implementation of this paper, YOLOv5 [40] is utilized after fine-tuning.

In assessing transmission efficiency, three metrics are employed: bit-rate (for lossless transmission), channel bandwidth ratio (CBR, for wireless transmission) and signal-to-noise ratio (for transmission through noisy channels). The bit-rate is calculated by dividing the total number of bits by the video duration. For reference frames in `val1` and `val2`, the average data amount of OAR are 366 bits and 219 bits, respectively. Utilizing a predictive coding approach, the average bit-rates of the OAR sequences are 3.5 kbps and 2.2 kbps, respectively.

CBR is defined as the ratio of the number of transmitted symbols to the original number of source symbols. For dataset `val1`, an additional CBR of 7.0×10^{-4} and 2.7×10^{-4} is expected for the OAR of reference frame and the overall video, respectively. For dataset `val2`, corresponding CBRs are 4.2×10^{-4} and 1.7×10^{-4} .

The signal-to-noise ratio SNR is the ratio of signal power P_S to noise power P_N . For an AWGN channel $N \sim G(0, \sigma^2)$, the SNR is expressed as $SNR(dB) = 10 \log_{10} P_S / \sigma^2$. Without loss of generality, $P_S = 1$ is adopted, i.e., both the emitting symbols of JSCC and the conventional method are power-normalized.

4) *Baselines and Comparison Algorithms*: For the proposed OAR-based video coding system, the performance is compared with conventional video codec H.265 and deep learning-based codec DVC [41]. The H.265 codec utilizes the `x265` implementation of `ffmpeg` [42], and the bit-rate is adjusted by CRFs. DVC is fine-tuned to achieve various bit-rates. Both pretrained

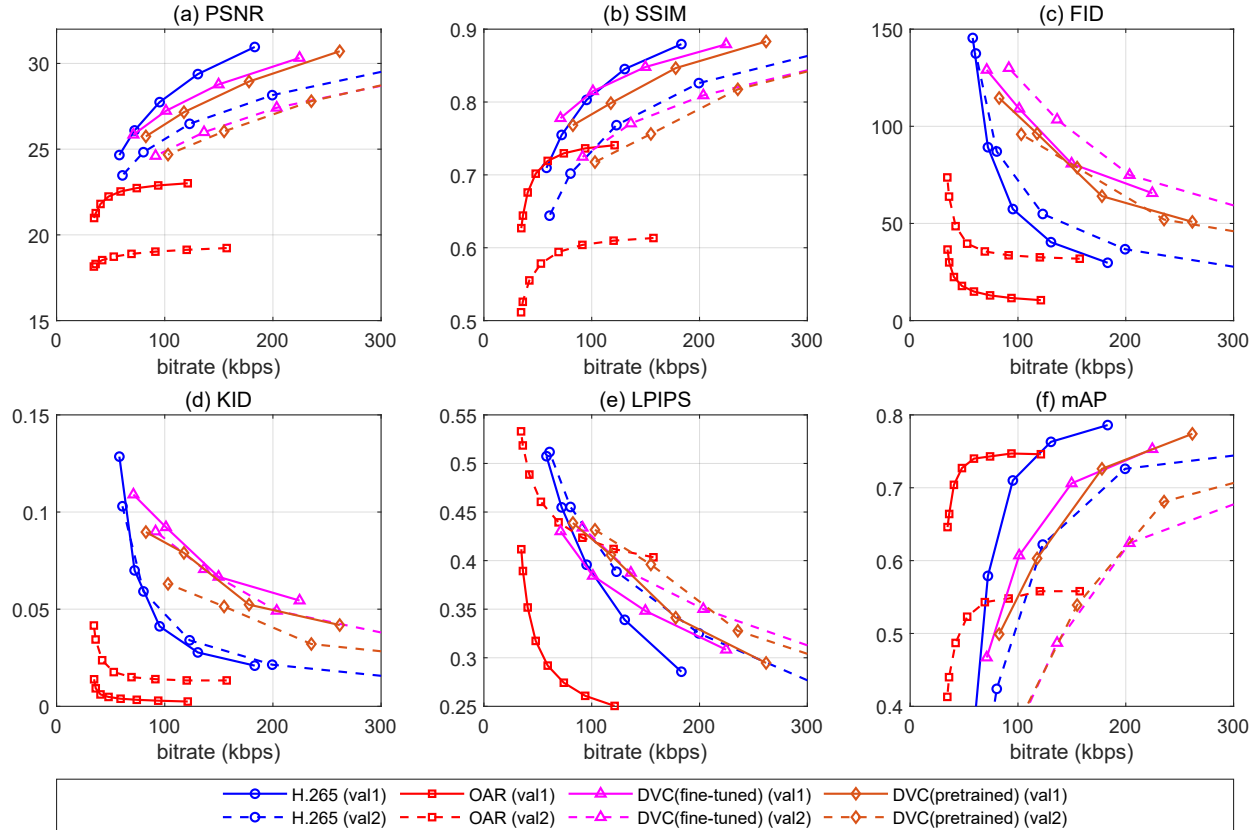


Fig. 5. The performance achieved by the proposed OAR based video coding method with H.265 and DVC at different bit-rates.

model (labeled by pretrained) and the one fine-tuned on UA-DETRAC (labeled by fine-tuned) are examined to mitigate the influence of dataset distribution.

For video transmission over AWGN channels, the experiments consist of transmission of reference frames and transmission of entire videos. For reference frames, the image undergoes encoding with BPG, followed by LDPC [33] coding, and modulation with either BPSK or QAM. BPG implementation is based on the open-source tool [35], while LDPC and BPSK/QAM modulation are adopted from [43]. Three parameter configurations of 1/3 rate (1536,4608) LDPC, 1/2 rate (3072,6144) LDPC and 2/3 rate (3072,4608) LDPC are examined for channel coding, while modulation schemes of BPSK, 4QAM, 16QAM and 64QAM are realized for symbol mapping. In addition, this paper compares the performance of the proposed OAR-based JSCC with the original model to assess the impact of OAR. Both JSCC models utilize identical training methods and network structures to ensure fairness in comparison.

Furthermore, the performance of OAR-based video transmission over AWGN channels is compared with H.265 video coding followed by LDPC and QAM. Besides, the recent video JSCC method DVST [9] is

implemented and compared. The DVST model is trained at SNR=10dB and fine-tuned with different rate control parameters to achieve lower CBRs.

B. Rate-Distortion Performance of OAR-Based Video Transmission System

Fig. 5 presents the performance comparison of the proposed OAR-based video coding with H.265 and DVC across different metrics on datasets `val1` (solid line) and `val2` (dashed line). From Fig. 5 (a) and (b), it's evident that OAR-based video coding is inferior to H.265 and DVC in terms of pixel fidelity. This is because that the proposed coding primarily focuses on downstream vision tasks, where detailed textures of the object and background are either provided by the reference frames or generated directly without rely on residuals. The discarding of prediction residuals plays a crucial role in achieving significant bit-rate reduction.

Despite the absence of residuals, the proposed method outperforms H.265 in terms of feature distribution and perceptual quality. As indicated from Fig. 5 (c) and (d), the proposed method better preserves the distribution properties in the feature dimension, leveraging prior information from trained parameters. Conversely, H.265

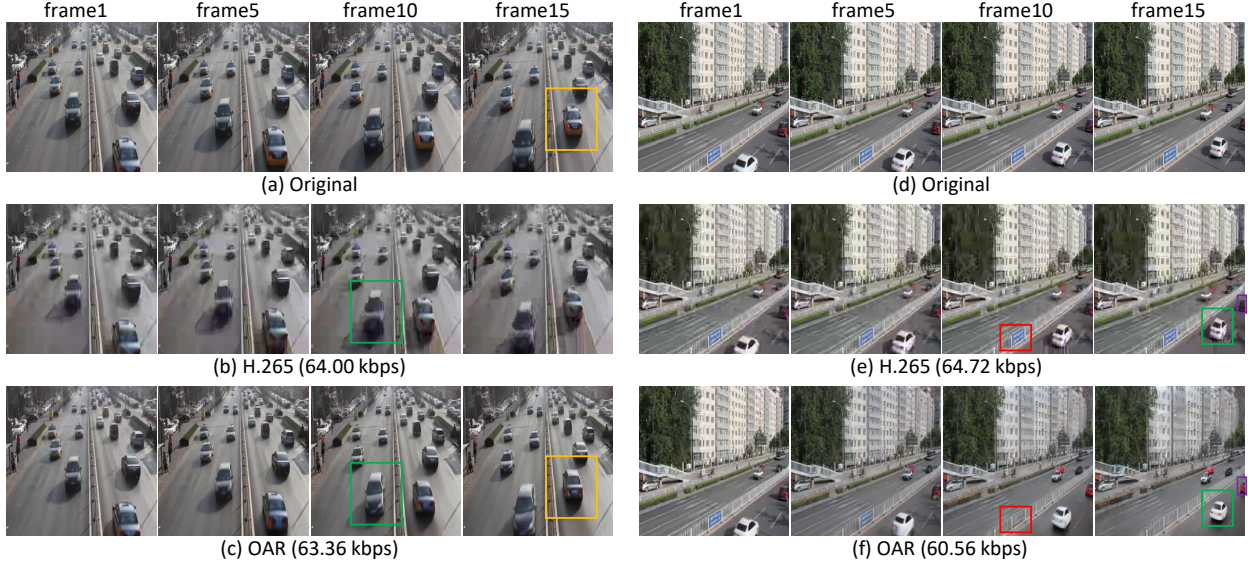


Fig. 6. Visualization of the reconstruction results achieved by different algorithms. (a)-(c) correspond to the `val11` dataset and (d)-(f) correspond to the `val12` dataset. The bit-rates achieved by H.265 and the proposed OAR-based methods are labeled.

exhibits significant feature bias due to the obvious block effect and blurring distortion at low bit-rates. Similarly, according to the LPIPS metrics demonstrated in Fig. 5 (e), the proposed method achieves superior perceptual quality at lower bit-rates (below 100 kbps).

Furthermore, as depicted in Fig. 5 (f), the proposed method maintains high object detection performance as the bit-rate decreases, reflecting the effective reconstruction of foreground objects by OAR. Conversely, H.265 experiences significant performance degradation when the bit-rate falls below 100 kbps. This is because the OAR contains vital object information, enabling better object recovery even at low bit-rates. Specifically, the position and category information within OAR provide object motion and appearance features in the reconstructed video. From another perspective, the OAR-based video coding method achieves 60.56% and 57.08% bit-rate savings when the average mAP reaches 0.7 (`val11`) or 0.4 (`val12`). The performance of DVC is inferior to H.265 in general. Furthermore, since DVC and H.265 share identical channel coding and transmission methods, the wireless transmission performance of DVC is not evaluated subsequently.

Fig. 6 displays video frames reconstructed by H.265 and OAR-based coding at a bit-rate of approximately 65 kbps. As shown in the figure, the proposed method significantly reduces the block effect, enhancing perceptual quality compared to H.265 (highlighted in green boxes). Furthermore, objects at edges are better preserved due to the object position and category information in the OAR (marked by purple boxes).

Comparison of `val11` and `val12` in Figure 5 reveals

that methods generally achieve lower performance on `val12`. This is primarily due to `val12` containing more complex motion patterns, posing challenges for inter-frame prediction and compensation. Moreover, `val12` contains more complex objects that are inherently harder to detect efficiently, leading to degraded object detection performance across all methods. Moreover, for OAR-based coding, the distribution disparity between `val12` and the training set also results in performance losses. As shown in Fig. 6, the object marked by the yellow box suffers from color deviation because the tail of the car is absent in the reference frame, while the background elements marked by the red box gradually fade. Despite this, in practical surveillance video applications, efficient adaptation through model fine-tuning is feasible, given the long processing period and relatively steady backgrounds. To ensure a fair performance comparison and mitigate the impact of the dataset distribution, subsequent analysis predominantly focuses on `val12`.

C. Performance Evaluation of OAR-assisted JSCC

1) *OAR-assisted Image JSCC for Reference Frame Transmission*: Performance of OAR-assisted JSCC is compared with BPG-based transmission and base JSCC for reference frame transmission. Fig. 7(a)-(b) depict the image LPIPS variation with SNR at different CBRs, while Fig. 7(c)-(d) illustrate the variation with the CBR at different SNRs. OAR-assisted JSCC generally outperforms base JSCC, particularly at high CBR (Fig. 7(b)) and low SNR (Fig. 7(c)). Specifically, compared to most BPG+LDPC+QAM schemes, OAR-assisted JSCC avoids cliff effects. It also surpasses

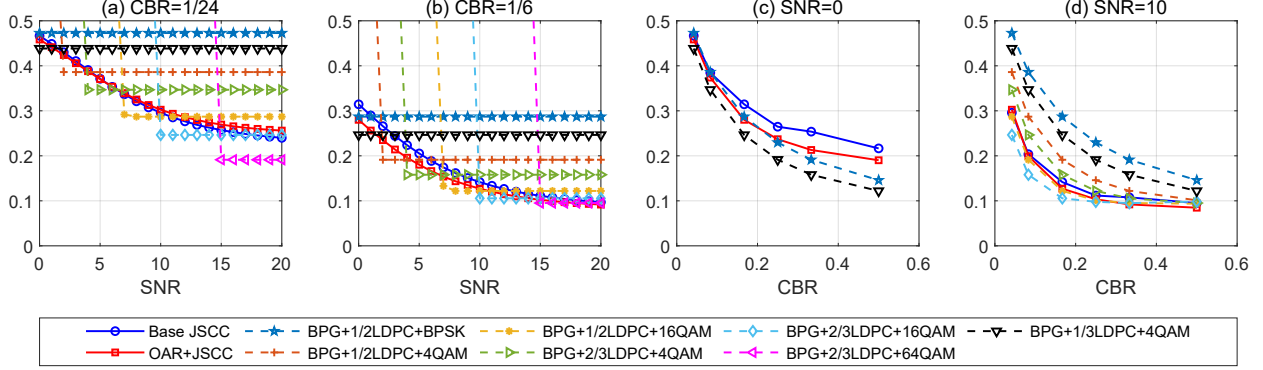


Fig. 7. The image perceptual quality (LPIPS) at different CBRs and SNRs. (a)-(b) illustrate the LPIPS versus SNR at different CBRs, and (c)-(d) illustrate the LPIPS versus CBR at different SNRs.

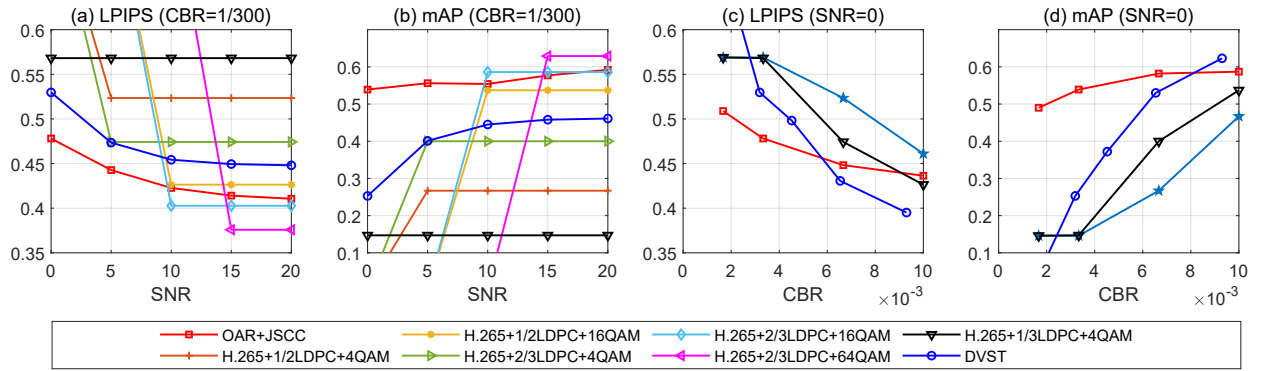


Fig. 8. Performance comparison of OAR-based video transmission to H.265 paired with LDPC and DVST. (a)-(b) are performances at CBR of 1/300, and (c)-(d) at SNR of 0 dB. The H.265-based transmission under some parameters suffer from decode failure and is not plotted.

BPG+1/3LDPC+4QAM and BPG+1/2LDPC+BPSK methods, which do not suffer from cliff effects in the 0~20 dB interval, particularly at high SNR (Fig. 7(b)). Furthermore, Fig. 7(c) demonstrates that OAR-assisted JSCC still maintains effective transmission at low SNR, while most BPG-based transmissions encounter truncation, failing to achieve effective transmission. Simultaneously, Fig. 7(d) highlights the superior performance of OAR-assisted JSCC at higher SNRs.

2) OAR-assisted Video Transmission through JSCC:

The overall performance of the proposed video transmission system, integrating OAR-based video coding and OAR-assisted JSCC, is assessed. Figure 8 compares the performance of the proposed OAR-based video transmission system with traditional H.265-based mechanisms and the deep JSCC method DVST [9]. Fig. 8(a) and (b) demonstrate the variations in perceptual quality (LPIPS) and downstream task performance (mAP) at a CBR of 1/300. The proposed OAR-based method demonstrates superior perceptual quality and task performance, particularly at low SNRs. While H.265-based video transmission exhibits better quality at higher SNRs, it suffers from the cliff effect. Notably, under a CBR constraint

of 1/300, the proposed method consistently outperforms DVST across all SNRs, achieving an average LPIPS loss reduction of 0.037 and mAP enhancement of 0.16.

Fig. 8(c) and (d) illustrate the variation in performances with CBR at a fixed SNR of 0 dB. It is evident that the proposed method achieves optimal perceptual quality and downstream task performance in the low CBR range (below 0.006). This is attributed to the capability to effectively reconstruct objects by leveraging explicit semantics of OAR and prior knowledge of the generative model. The performance improvement of our proposed method is comparatively gradual with increasing CBR compared to other methods. This is because other methods achieve video quality enhancement by transmitting residuals. Hence, our method is better suitable for environments with severely limited bandwidth and significant noise interference.

V. ANALYSIS, DISCUSSIONS AND ABLATION STUDIES

A. Appearance Enhancement with Semantic Priors

Experiments conducted on OAR-based video coding at low bit-rates reveal that the proposed video generation

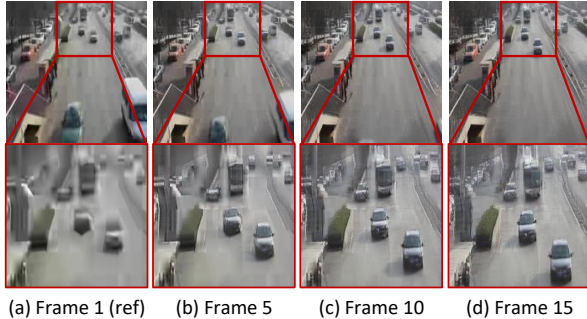


Fig. 9. The video reconstruction results with reference frames of poor quality. The reference frame is taken as CRF 48.

TABLE I
VARIATION OF mAP ACHIEVED BY WARMUP OPERATION

dataset	CRF of reference frame					
	48	45	42	39	36	33
val1	0.020	0.008	-0.017	-0.026	-0.035	-0.036
val2	0.022	0.011	-0.012	-0.037	-0.051	-0.050

model effectively enhances reconstruction of objects using semantic priors. Illustrated in Fig. 9, this effect is demonstrated by showing the 5th, 10th, and 15th frames of the reconstructed video alongside their corresponding local details. It is evident that the reconstruction model progressively incorporates prior information from the training set into the reconstructed frames, resulting in enhanced object details.

Accordingly, we propose a warm-up strategy to further validate the effectiveness of the prior knowledge. Specifically, we use the compressed first frame as the reference frame and use the corresponding OAR for image generation. The above process is repeated for several iterations, with each generated image serving as the reference frame for the next iteration, which is called the warm-up stage. Subsequent frames are then generated after completing the warm-up stage. Table I presents the variations in mAP with warm-up of 10 iterations on the `val1` and `val2` datasets. It is observed that warm-up at low bit-rates enhances the video quality to a certain extent. However, when the reference frames exhibit good quality (with CRF values of 42 and above), excessive inference by the model results in the loss of original details, leading to degradation of video quality.

B. Ablation Studies for OAR Attributes and Relations

To assess the influence of each element in OAR, ablation experiments are conducted across three dimensions: object categories, orientations, and relations. In each experiment, the same model is utilized for video generation, with different alterations to the OAR sequences: (1) `w/o category`: setting all categories to “car”; (2) `w/o`



Fig. 10. Visualization of ablation experiments. (a) Real image; (b) Reference frame; (c) Original reconstructed frame; (d) Reconstructed frame of ablation setting: `w/o category`; (e) Reconstructed frame of ablation setting: `w/o angle`. The bottom halves of (d) and (e) are the same as those in (c).

TABLE II
AVERAGE VARIATIONS IN MAP METRICS OF VIDEOS OBTAINED BY DIFFERENT ABLATION METHODS

phase	<code>w/o category</code>	<code>w/o angle</code>	<code>w/o relation</code>
val1	-0.108	-0.059	-0.001
val2	-0.105	-0.052	-0.001

`angle`: fixing all angles to 0; (3) `w/o relation`: removing all occlusion relations. The performance variation in mAP is shown in Table II. As indicated from the table, object category and angle produce significant impact on reconstruction performance, whereas relation has minimal impact. This suggests that occlusion relations may be implicitly embedded in spatial locations due to the independence of objects, rendering them redundant in the OAR. However, the inclusion of relations in OARs ensures the integrity of the graph structure, facilitating the adaptation and expansion of OAR representations to more complex scenes.

Fig. 10 demonstrates further video reconstruction results from the ablation experiments (1) and (2). As shown in Fig. 10 (a) to (c), the van absent in the reference frame is generated leveraging category information from the OAR, and is correctly recognized as a “van” with high confidence. This indicates the adaptability of OAR-based video transmission to downstream tasks. While in Fig. 10(d), mislabeling the category as “car” results in car-like appearances, such as a black body and a smaller front end. However, the bus in the upper-left corner, primarily influenced by appearance information from the reference frame, remains unaffected by OAR mislabeling. This reflects the capability of OAR to explicitly govern video semantics, suggesting its potential application in diverse domains like video editing and privacy protection. Fig. 10(e) demonstrates the rectification of the model for angle mislabeling. This suggests the angle’s impact on object appearance is not as pronounced as category, manifesting instead through a composite effect with background or other features. On the other hand, this also indicates that the object orientation is also concurrently influenced by motion.

From the above analysis, it is evident that the attributes of object categories have explicit influence on appearance. To delve deeper into the interplay between categories, the impact of category mislabeling on various objects is examined. Experiments show that the average precision of “van” decreases by 0.316 and 0.340 on val1 and val2, respectively, while “bus” and “others” have relatively minor variations.

Objects categorized as “bus” and “others” exhibit less susceptibility to category mislabeling due to their distinct sizes and movement patterns compared to cars. Conversely, vans are most affected by mislabeling, with nearly half of originally correctly recognized objects (with mean mAPs of 0.643 and 0.484 for val1 and val2, respectively) being misidentified. Further experiments reveal that after being mislabeled as car, the proportion of vans misidentified as cars increases from 35% to 67%. This indicates that objects with similar appearances are more susceptible to category labeling. This further exemplifies the explicit role of OAR in semantics and inspires awareness of distinctiveness among different attributes during labeling design.

C. Performance Variants for OAR-assisted JSCC

Fig. 11 compares the LPIPS versus SNR performances of OAR-assisted JSCC with the base JSCC. At low CBRs (e.g., CBR=1/24), OAR-assisted JSCC does not outperform base JSCC, particularly at high SNRs. However, as CBR increases, OAR-assisted JSCC surpasses base JSCC, presenting a significant advantage. This is attributed to the increased number of output channels in the network, allowing more OAR prior information to be reflected in transmitted symbols and facilitating efficient decoding at the receiver. In fact, given that downstream tasks prioritize perceptual and semantic considerations, it is more valuable to optimize the loss function from perceptual and semantic perspectives [44], [45]. However, since this paper primarily focuses on video transmission with OAR as auxiliary information, refining the JSCC model specifically for reference frames falls outside the scope of this study.

VI. CONCLUSION

In this paper, an OAR-assisted video coding and transmission method was proposed to address the challenge of efficient and reliable video transmission for downstream tasks. First, an OAR-based video representation and coding system was proposed to realize a low bit-rate representation of videos by object-attribute-relation (OAR). Second, a generative video reconstruction method based on reference frames and OAR sequences was implemented to realize perceptual-quality and downstream-task oriented reconstruction. Finally, OAR-assisted JSCC

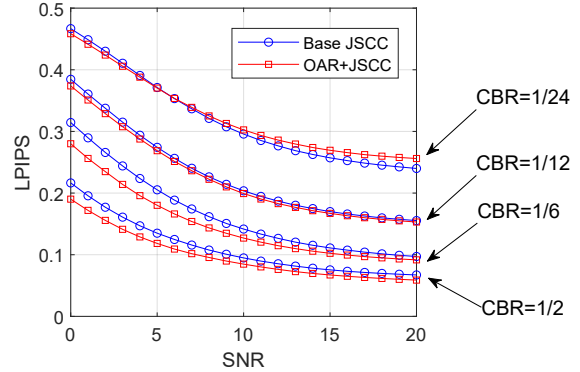


Fig. 11. The PSNR versus SNR curves of the foreground region obtained by different JSCC models for the three CBR values.

was proposed and combined with OAR-based video coding to realize video transmission in noisy channels. Experiments on a traffic surveillance dataset demonstrated the effectiveness of our approach. First, the proposed OAR-based video coding outperformed H.265 in terms of perceptual quality and downstream object detection performance and saved up to 61% bit-rate. Second, the implemented OAR-based video transmission system could be adaptable to low bandwidth and SNR conditions, effectively ensuring perceptual quality and downstream task performance. At a CBR of 1/300, our method achieved an average LPIPS loss reduction of 0.037 and object detection performance (mAP) improvement of 0.16 compared to DVST. Additionally, the scalability of the proposed OAR representation suggests its potential applicability in complex scenarios such as border and sea defense, as well as applications requiring explicit semantic control like privacy-preserving video transmission.

REFERENCES

- [1] J. Li, B. Li, and Y. Lu, “Deep contextual video compression,” *Adv. Neural Inf. Process. Syst.*, vol. 34, pp. 18 114–18 125, 2021.
- [2] E. Bourtsoulatze, D. Burth Kurka, and D. Gündüz, “Deep joint source-channel coding for wireless image transmission,” *IEEE Transactions on Cognitive Communications and Networking*, vol. 5, no. 3, pp. 567–579, 2019.
- [3] C. E. Shannon and W. Weaver, “The mathematical theory of communication,” *Philosophical Review*, vol. 60, no. 3, 1949.
- [4] D. Gündüz, Z. Qin, I. E. Aguerri, H. S. Dhillon, Z. Yang, A. Yener, K. K. Wong, and C.-B. Chae, “Beyond transmitting bits: Context, semantics, and task-oriented communications,” *IEEE Journal on Selected Areas in Communications*, vol. 41, no. 1, pp. 5–41, 2023.
- [5] H. Xie, Z. Qin, G. Y. Li, and B.-H. Juang, “Deep learning enabled semantic communication systems,” *IEEE Transactions on Signal Processing*, vol. 69, pp. 2663–2675, 2021.
- [6] L. Yan, Z. Qin, R. Zhang, Y. Li, and G. Y. Li, “Resource allocation for text semantic communications,” *IEEE Wireless Communications Letters*, vol. 11, no. 7, pp. 1394–1398, 2022.
- [7] Z. Weng and Z. Qin, “Semantic communication systems for speech transmission,” *IEEE Journal on Selected Areas in Communications*, vol. 39, no. 8, pp. 2434–2444, 2021.

- [8] D. Huang, F. Gao, X. Tao, Q. Du, and J. Lu, "Toward semantic communications: Deep learning-based image semantic coding," *IEEE Journal on Selected Areas in Communications*, vol. 41, no. 1, pp. 55–71, 2023.
- [9] S. Wang, J. Dai, Z. Liang, K. Niu, Z. Si, C. Dong, X. Qin, and P. Zhang, "Wireless deep video semantic transmission," *IEEE Journal on Selected Areas in Communications*, vol. 41, no. 1, pp. 214–229, 2023.
- [10] T. Han, Q. Yang, Z. Shi, S. He, and Z. Zhang, "Semantic-preserved communication system for highly efficient speech transmission," *IEEE Journal on Selected Areas in Communications*, vol. 41, no. 1, pp. 245–259, 2022.
- [11] Q. Du, Y. Duan, Z. Xie, X. Tao, L. Shi, and Z. Jin, "Optical flow-based spatiotemporal sketch for video representation: A novel framework," *IEEE Transactions on Circuits and Systems for Video Technology*, 2024.
- [12] M. Yang and H.-S. Kim, "Deep joint source-channel coding for wireless image transmission with adaptive rate control," in *ICASSP 2022 - 2022 IEEE International Conference on Acoustics, Speech and Signal Processing (ICASSP)*, 2022, pp. 5193–5197.
- [13] M. Yang, C. Bian, and H.-S. Kim, "Deep joint source channel coding for wireless image transmission with ofdm," in *JCC 2021 - IEEE International Conference on Communications*, 2021, pp. 1–6.
- [14] T.-Y. Tung and D. Gündüz, "Deepwive: Deep-learning-aided wireless video transmission," *IEEE Journal on Selected Areas in Communications*, vol. 40, no. 9, pp. 2570–2583, 2022.
- [15] W. Zhang, H. Zhang, H. Ma, H. Shao, N. Wang, and V. C. M. Leung, "Predictive and adaptive deep coding for wireless image transmission in semantic communication," *IEEE Transactions on Wireless Communications*, vol. 22, no. 8, pp. 5486–5501, 2023.
- [16] C. Li, Y. Duan, Q. Du, S. Sun, X. Deng, and X. Tao, "Vr+hd: Video semantic reconstruction from spatio-temporal scene graphs," *IEEE Journal of Selected Topics in Signal Processing*, 2023.
- [17] A. Bassiouny and M. El-Saban, "Semantic segmentation as image representation for scene recognition," in *2014 IEEE International Conference on Image Processing (ICIP)*, 2014, pp. 981–985.
- [18] J. Ji, R. Krishna, L. Fei-Fei, and J. C. Niebles, "Action genome: Actions as compositions of spatio-temporal scene graphs," in *Proceedings of the IEEE/CVF Conference on Computer Vision and Pattern Recognition*, 2020, pp. 10236–10247.
- [19] T.-C. Wang, M.-Y. Liu, J.-Y. Zhu, G. Liu, A. Tao, J. Kautz, and B. Catanzaro, "Video-to-video synthesis," in *Advances in Neural Information Processing Systems (NeurIPS)*, 2018.
- [20] A. Bar, R. Herzig, X. Wang, A. Rohrbach, G. Chechik, T. Darrell, and A. Globerson, "Compositional video synthesis with action graphs," in *Proceedings of the 38th International Conference on Machine Learning*, ser. Proceedings of Machine Learning Research, M. Meila and T. Zhang, Eds., vol. 139. PMLR, 18–24 Jul 2021, pp. 662–673. [Online]. Available: <https://proceedings.mlr.press/v139/bar21a.html>
- [21] D. Huang, X. Tao, F. Gao, and J. Lu, "Deep learning-based image semantic coding for semantic communications," in *2021 IEEE Global Communications Conference (GLOBECOM)*, 2021, pp. 1–6.
- [22] M. Akbari, J. Liang, and J. Han, "Dsslic: Deep semantic segmentation-based layered image compression," in *ICASSP 2019 - 2019 IEEE International Conference on Acoustics, Speech and Signal Processing (ICASSP)*, 2019, pp. 2042–2046.
- [23] E. Grassucci, S. Barbarossa, and D. Comminiello, "Generative semantic communication: Diffusion models beyond bit recovery," *arXiv preprint: arXiv:2306.04321*, 2023.
- [24] P. Jiang, C.-K. Wen, S. Jin, and G. Y. Li, "Wireless semantic communications for video conferencing," *IEEE Journal on Selected Areas in Communications*, vol. 41, no. 1, pp. 230–244, 2023.
- [25] Z. Zhang, Q. Yang, S. He, and J. Chen, "Deep learning enabled semantic communication systems for video transmission," in *2023 IEEE 98th Vehicular Technology Conference (VTC2023-Fall)*, 2023, pp. 1–5.
- [26] Z. Bao, H. Liang, C. Dong, X. Xu, and G. Liu, "Mdvsc—wireless model division video semantic communication for 6g," in *2023 IEEE Globecom Workshops (GC Wkshps)*, 2023, pp. 1572–1578.
- [27] W. Gong, H. Tong, S. Wang, Z. Yang, X. He, and C. Yin, "Adaptive bitrate video semantic communication over wireless networks," in *2023 International Conference on Wireless Communications and Signal Processing (WCSP)*, 2023, pp. 122–127.
- [28] C.-Y. Wang and H.-Y. M. Liao, "YOLOv9: Learning what you want to learn using programmable gradient information," *arXiv*, 2024.
- [29] A. Bewley, Z. Ge, L. Ott, F. Ramos, and B. Upcroft, "Simple online and realtime tracking," in *2016 IEEE International Conference on Image Processing (ICIP)*, 2016, pp. 3464–3468.
- [30] S. Li, Z. Yan, H. Li, and K.-T. Cheng, "Exploring intermediate representation for monocular vehicle pose estimation," in *Proceedings of the IEEE/CVF Conference on Computer Vision and Pattern Recognition (CVPR)*, June 2021, pp. 1873–1883.
- [31] T. Mikolov, I. Sutskever, K. Chen, G. Corrado, and J. Dean, "Distributed representations of words and phrases and their compositionality," in *Proceedings of the 26th International Conference on Neural Information Processing Systems - Volume 2*, ser. NIPS'13. Red Hook, NY, USA: Curran Associates Inc., 2013, p. 3111–3119.
- [32] T. N. Kipf and M. Welling, "Semi-supervised classification with graph convolutional networks," in *International Conference on Learning Representations (ICLR)*, 2017.
- [33] R. Gallager, "Low-density parity-check codes," *IRE Transactions on Information Theory*, vol. 8, no. 1, pp. 21–28, 1962.
- [34] L. Wen, D. Du, Z. Cai, Z. Lei, M.-C. Chang, H. Qi, J. Lim, M.-H. Yang, and S. Lyu, "Ua-detrac: A new benchmark and protocol for multi-object detection and tracking," *Computer Vision and Image Understanding*, vol. 193, p. 102907, 2020. [Online]. Available: <https://www.sciencedirect.com/science/article/pii/S1077314220300035>
- [35] F. Bellard, "Better portable graphics," <https://bellard.org/bpg/>, 2018.
- [36] R. Zhang, P. Isola, A. A. Efros, E. Shechtman, and O. Wang, "The unreasonable effectiveness of deep features as a perceptual metric," in *2018 IEEE/CVF Conference on Computer Vision and Pattern Recognition*, 2018, pp. 586–595.
- [37] M. F. Naeem, S. J. Oh, Y. Uh, Y. Choi, and J. Yoo, "Reliable fidelity and diversity metrics for generative models," in *International Conference on Machine Learning*, 2020.
- [38] M. Bińkowski, D. J. Sutherland, M. Arbel, and A. Gretton, "Demystifying MMD GANs," in *International Conference on Learning Representations*, 2018. [Online]. Available: <https://openreview.net/forum?id=r1UOzWCW>
- [39] A. Obukhov, M. Seitzer, P.-W. Wu, S. Zhydenko, J. Kyl, and E. Y.-J. Lin, "High-fidelity performance metrics for generative models in pytorch," 2020, version: 0.3.0. [Online]. Available: <https://github.com/toshas/torch-fidelity>
- [40] G. Jocher, "Yolov5 by ultralytics," 2020. [Online]. Available: <https://github.com/ultralytics/yolov5>
- [41] G. Lu, W. Ouyang, D. Xu, X. Zhang, C. Cai, and Z. Gao, "Dvc: An end-to-end deep video compression framework," in *Proceedings of the IEEE/CVF Conference on Computer Vision and Pattern Recognition*, 2019, pp. 11006–11015.
- [42] F. Developers, "ffmpeg tool," 2016. [Online]. Available: <http://ffmpeg.org/>
- [43] H. Yoo, L. Dai, S. Kim, and C.-B. Chae, "On the role of vit and cnn in semantic communications: Analysis and prototype validation," *IEEE Access*, vol. 11, pp. 71528–71541, 2023.
- [44] E. Erdemir, T.-Y. Tung, P. L. Dragotti, and D. Gündüz, "Generative joint source-channel coding for semantic image transmission," *IEEE Journal on Selected Areas in Communications*, vol. 41, no. 8, pp. 2645–2657, 2023.
- [45] J. Wang, S. Wang, J. Dai, Z. Si, D. Zhou, and K. Niu, "Perceptual learned source-channel coding for high-fidelity image semantic transmission," 2022.